Hydrogen Trapping in X70 Structural Pipeline Steel and Weldments

Jean-Gabriel Sezgin[a], Hallvard G. Fjær[b], Hisao Matsunaga[c,d,e], Junichiro Yamabe[a,c,f], Vigdis Olden[g]

[a]AIST-Kyushu University Hydrogen Materials Laboratory (HydroMate), National Institute of Advanced Industrial Science and Technology (AIST), Fukuoka, Japan
[b]Institute for Energy Technology, Kjeller, Norway
[c]Research Center for Hydrogen Industrial Use and Storage (HYDROGENIUS), Kyushu University, Fukuoka, Japan
[d]Department of Mechanical Engineering, Kyushu University, Fukuoka, Japan
[e]International Institute for Carbon-Neutral Energy Research (I2CNER), Kyushu University, Fukuoka, Japan
[f]International Research Center for Hydrogen Energy, Kyushu University, Fukuoka, Japan
[g]SINTEF, Department of Materials and Nanotechnology, Trondheim, Norway

ABSTRACT

Diffusion measurements and thermal desorption measurements have been performed on a X70 pipeline steel, in as received and normalized and quenched condition, after being hydrogen charged for 200 h at 100 MPa hydrogen gas pressure and 85℃. Numerical simulations based on the assumption of thermodynamic equilibrium were performed, aiming to compare the trapping energies when fitting to the TDS spectra. TDS experiments revealed a reversible trap site with activation energy of 26.2 kJ.mol^{-1}. Irreversible trap sites with an activation energy of >100 kJ.mol^{-1} were observed from both as-received and heat-treated condition. In contrast, a reversible trap site with an activation energy of 49.2 kJ.mol^{-1} was observed only from the heat-treated condition. The numerical modelling based on the assumption of equilibrium between hydrogen in traps and hydrogen in lattice is seen to provide a good fit to the experimental data.

KEY WORDS: Steel; pipeline; weld; hydrogen; embrittlement; trapping; desorption

INTRODUCTION

Subsea oil and gas structural steel pipelines are exposed to hydrogen at the steel surface due to cathodic protection towards corrosion. Hydrogen reduces the fracture toughness in the base metal as well as in welded joints, which may be critical for the structural integrity of the pipeline. As atomic hydrogen enters the steel it occupies lattice sites and traps, as dislocations, grain boundaries and precipitates, often categorized as reversible and irreversible traps according to their trapping energy.
To be able to build predictive models for the fracture susceptibility of pipelines under operation conditions, knowledge of the amount of diffusible hydrogen and trapped hydrogen that may contribute to fracture, are vital information. Thus, knowledge of the trapping energies is essential.

In the present work, results from Thermal Desorption Spectrometry (TDS) measurements of X70 structural steel will be presented. As-received steel and heat-treated (normalized and quenched) steel, representative of the coarse grain heat affected zone of a welded joint, are investigated. Finally, the measured trapping energies, diffusivity and hydrogen concentration are discussed and compared to a numerical model, where the trapping energies are assessed.

MATERIAL

The investigated material is an API grade X70 structural pipeline steel. Table 1 shows the chemical composition.

Table 1 Chemical composition of the X70 pipeline steel (wt%).

	C	Mn	Si	P	S	Cu	Ni
API X70	0.047	1.74	0.1	001	0.007	0.22	0.25
	Al	Nb	V	Cr	Mo	Ti	N
	0.027	0.027	0.001	0.047	0.042	0.01	0.0025

The yield ($R_{p0.2}$) and ultimate tensile properties (R_m) are 485 MPa and 600 MPa in the as-received condition and 643 MPa and 830 MPa for the heat-treated condition. All in the rolling direction of the plate. Heat-treatment is performed by normalizing treatment for 35 minutes at 1280°C, followed by direct water quenching aiming to obtain a microstructure representative of the coarse-grained heat affected zone in a welded joint.

Representative microstructures before and after heat treatment are presented in Figure 1. Figure 1 a, shows that the as-received micro-structure mainly consists of banded fine-grained ferrite with less than 5 % globular pearlite. After quenching, the microstructure is a mix of martensite and bainite, Figure 1b.

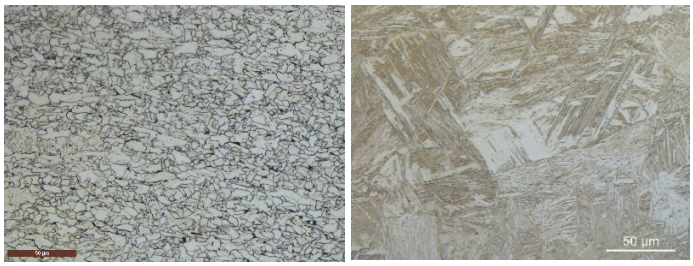

Figure 1 Representative API X70 Micro structure a) As received b) Normalized and quenched

DIFFUSION AND TRAPPING PROPERTIES FROM TDS MEASUREMENT

Sample preparation and hydrogen charging

Two experimental protocols are considered to obtain the diffusion and trapping properties of the steel. The measurements of hydrogen diffusivity and TDS rely on distinct specimen geometries. The specimens are charged in high-pressure hydrogen gas prior to the measurements. The hydrogen charging here consists in the exposure of the specimens to 100 MPa hydrogen gas at 85℃ during 200 h. These conditions ensure the flat profile of hydrogen concentration across the specimens, based on the knowledge of the laboratory. Such experiment could be used afterward to provide an approximate value of the effective concentration of hydrogen in solution in the steel.

The samples for the diffusivity measurements are 15 mm long cylindrical specimens with a diameter of 15 mm. The surface of the specimens has been processed by #600 emery paper. Some previous studies conducted on various low alloy steels as well as austenitic stainless steels have proved that the surface finished by buff polishing with #2000 media does not enhance neither the accuracy nor the reproductivity of the measurement procedure; in a context of hydrogen desorption based experiments (Yamabe et al, 2017). In parallel, it is well known that surface oxidation may affect the adsorption of hydrogen at a metallic surface (Yamabe et al, 2015). However, the effects issued from surface oxidation tend to become significant near room temperature. Therefore, in the present work, only the measurement performed near room temperature involves deposition of Pd which the thickness on the order of few nanometers to the surface by means of ion-sputtering technique. This point is emphasized by the excellent coherence of the obtained results whether the specimens were coated by Pd or not, showing good agreement between measured values and the fitting by an Arrhenius law. In addition, these specimens are usually thick since the measured phenomena must be diffusion controlled.

The samples related to the TDS measurements have followed the same preparation protocol. However, this test must be based on desorption phenomena. The specimen geometry has therefore been modified to mitigate diffusive effects. The diameter is now 19 mm for a thickness of 2 mm.

Methods of determination

Diffusivity measurements

The diffusivity measurements consist in the analysis of the transient evolution of the hydrogen content within the specimen during desorption. More specifically, this parameter is calculated by fitting the experimental curve of residual hydrogen in the specimen according to an approximated analytical solution of the Fick equation. This expression links the residual content of hydrogen in the specimen to various parameters such as the desorption time, the diffusivity and the dimensions of the specimen. It is then straightforward to deduce the actual diffusivity experimentally. The desorption properties are measured by the measurement system equipped with gas chromatography mass-spectrometry (GC-MS). To retrieve the data required to calculate the Arrhenius' parameters, the system is kept at several constant temperatures. The whole fitting procedure as well as the development of the expressions could be found detailed in (Yamabe et al. 2015b). In this work, after the measurements at several constant temperatures, the remaining hydrogen content is measured under a rising temperature (TDS measurement) in order to gain insight on the trapping properties of the specimen without lattice hydrogen.

TDS measurements

The TDS consists in the measurement of the desorbed amount of hydrogen depending on both time and temperature. Assuming that the hydrogen can be trapped by crystallographic defects, and that the occupancy of the trapping sites is thermodynamically controlled, the trapping and release phenomena are consequently characterizable by an activation energy (trapping energy). In this case, the energy required to release trapped hydrogen is supplied by the temperature. The application of a constant temperature ramp will therefore provide a temperature dependent desorption spectrum. Consequently, the hydrogen release energy can be calculated based on the position of the peaks of desorption. Several methods have been established to analyze such spectra. The energies have been calculated using the Choo-Lee's method, leading to the following expression:

$$\frac{\partial\left[\ln\left(\frac{T_p^2}{\alpha}\right)\right]}{\partial\left(\frac{1}{T_p}\right)} = \frac{E_a}{R} \quad (1)$$

where α is the heating rate, T_p is the peak temperature and E_a is the activation energy of the considered trap. In the present work, it has been chosen on the one hand to perform the diffusivity and TDS measurements successively. On the other hand, some single TDS measurements on separate specimens of smaller dimensions are also performed. In the first case, a constant heating rate after holding at several constant temperatures (50℃, 100℃, 170℃) is applied, whereas in the latter case, no temperature holdings are applied. Depending on the holding, it is expected that the desorption of hydrogen from lattice or low-energy traps will occur. The main target of this post holding TDS measurement is to gain some visibility in case of contribution of multiple traps with close energies. In other words, the temperature holding enable a distinction between the different trapping energies by completely releasing the hydrogen contained in the lower- energy traps at first. Otherwise, the resulting signal is a convolution of several Gaussian distributions and must be deconvoluted to accurately access the trapping energies.

It is important to mention that the desorption spectra resulting from diffusivity measurements does not aim to provide a quantitative interpretation of the trapping energies because of the specimen dimensions. It can only be used to provide qualitative evidences as described further.

Results

Behavior of the hydrogen in solution

The results of the diffusivity measurements for both as-received and heat-treated conditions of the API X70 steel are presented in Figure 2. The diffusivities have been measured at four temperatures: 30℃, 50℃, 100℃, 170℃. The hydrogen diffusivities of the as-received condition are presented by blue circles whereas those of the heat-treated condition are represented by red diamond-shaped marks. The plot emphasizes a slightly larger diffusivity for the as-received condition than the heat-

treated one. The results of the fitting by an Arrhenius' law for each steel are drawn in solid and dashed lines respectively. Table 2 sums up the Arrhenius' coefficients of both steels fitted from the experimental results.

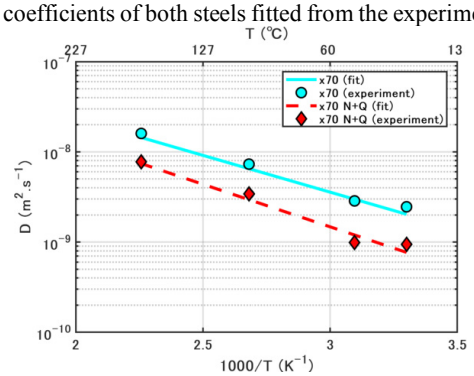

Figure 2 Arrhenius plots of measured diffusivity of the API X70 steels. Data of the as-received condition are represented by blue line and round markers and those of the heat-treated condition are represented by red dashed line and diamond-shaped markers.

Table 2 Approximated parameters involved in the Arrhenius' law for both conditions of the API X70 steel

	API X70	API X70 (N+Q)
Pre-exponential factor ($m^2.s^{-1}$)	1.10×10^{-6}	1.06×10^{-6}
Energy ($kJ.mol^{-1}$)	15.6	18.1

TDS experiments has been performed after the diffusivity measurements. Results of the as-received and heat-treated conditions are given by Figure 3 and Figure 4, respectively. The heating rate of the TDS specimens is 100℃.h^{-1}, regardless the case in consideration. Figure 3 shows the desorption spectra of the as-received condition. The peaks located at a lower temperature are related to both low-energy traps (also called reversible traps) and lattice diffusion, whereas the peaks located at a higher temperature is related to irreversible traps. It could be observed that for the TDS spectrum obtained from the specimen tested immediately after the hydrogen exposure (triangle markers, reference spectrum), only two peaks are present. The first one is related to hydrogen contained in the lattice and low-energy traps. To state the contribution of the lattice and traps to the desorption, the observation of the other spectra is required. Taking into consideration the other datasets, the spectra are identical to the reference one (it is considered that the specimens are tested few minutes after hydrogen exposure, because of the storage in liquid nitrogen) during temperature increase until reaching the targeted temperature for holding. Then, the holdings at constant temperatures cause hydrogen desorption. The desorption measurement under the constant temperatures is continued until reaching almost zero hydrogen detected, which means that all the hydrogen contained within the lattice and the low-energy traps has completed to be desorbed during the temperature holding. Beyond 360°C, the signal corresponds to the release of the hydrogen contained in higher-energy traps (i.e. irreversible traps). In the present desorption spectra, no signal is detected between holding temperatures (50, 100, and 170℃) and 360℃, which means that no reversible traps are observed. Moreover, the comparison of the shape of the signals at lower and higher temperatures suggests that multiple traps are present at a higher temperature. In general, the desorption peak is described by a Gaussian density. The neat distortion of the desorption Gaussian indicates that the contents of hydrogen trapped at these sites are not negligible; therefore, these irreversible traps must be present at comparable contents. In contrast, the shape of the desorption Gaussian does not ensure that no additional reversible traps are present at lower amount. In this case, the "no reversible trap" information is translated by the fact that no signal is detected after the holdings at constant temperatures.

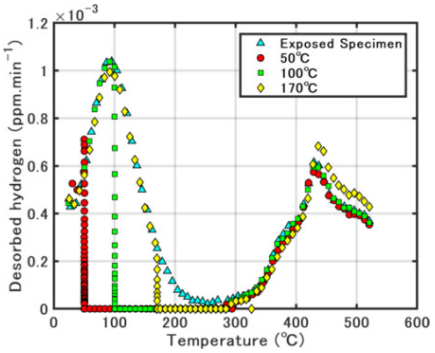

Figure 3 TDS spectra of the as-received condition. The TDS is performed under four testing conditions, after exposure to 100 MPa hydrogen gas at 85°C during 200 h.

In parallel, the time integration of the signal provides the access to the ratio of hydrogen contained in lattice/reversible traps to that in irreversible traps as well as the overall hydrogen content of the steel. The quantification regarding the as-received condition is provided by Table 3. The data contained in this table is nearly equal for each case, pointing out the reproducibility of the tests under various conditions. The total hydrogen content of the specimen being approximately 0.11 mass ppm, the proportion of hydrogen in the irreversible sites is 41%.

Table 3 Amount of hydrogen contained in the as-received steel for four test conditions.

	Holding temperature	50℃	100℃	170℃
Marker in Fig 3.	Triangle	Circle	Square	Diamond
Lattice/reversible	0.07	0.06	0.07	0.06
Irreversible	0.05	0.04	0.04	0.05
Total	0.12	0.10	0.11	0.11

The results of the TDS measurements performed on the heat-treated condition are summarized in Figure 4. The statements issued for the as-received condition remain mostly valid for the heat-treated one. Because the heating rate is constant, the observation of the area under the curve suggests that the hydrogen in solution is mostly contained in lattice and reversible traps rather than in irreversible ones. However, the difference in this case consists in the appearance of a secondary peak around 171℃ (as read on the curve for the temperature holding at 50℃, represented by red dots on the figure below). Because the temperature holding at 50℃ and higher are performed until reaching a desorption rate of near 0 mass ppm.min^{-1}, there is no contribution of the hydrogen in solution within the lattice to this secondary peak.

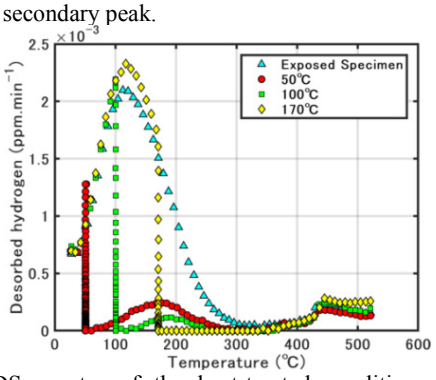

Figure 4 TDS spectra of the heat-treated condition. The TDS is performed for four testing conditions, after exposure to 100 MPa high pressure hydrogen at 85°C during 200h.

In the same manner, a quantitative measurement of the hydrogen in solution according to its position in the steel has been performed using the time-dependent data of the TDS measurements. The amount of hydrogen in each location is resumed in Table 4. For the heat-treated condition, the averaged total content of hydrogen is 1.9 times higher than that for the as-received condition. It could be also noteworthy that, in this case, the data issued from each case are nearly equal. However, the main fact is the proportion of hydrogen located in the irreversible part which is now reduced to 6.0%.

Table 4 Amount of hydrogen contained in the heat-treated condition for four testing conditions.

	Holding temperature	50℃	100℃	170℃
Marker in Fig 4.	Triangle	Circle	Square	Diamond
Lattice/reversible	0.18	0.20	0.20	0.20
Irreversible	0.01	0.01	0.01	0.02
Total	0.19	0.21	0.21	0.22

Trapping energies

To determine quantitatively the trapping properties of hydrogen in solution in the steel, TDS experiments have been performed. The results of these tests are given by Figure 5 and Figure 6. For the as-received condition, Figure 5 shows the results obtained from the as-received condition for three heating rates (50℃.h^{-1}, 100℃.h^{-1}, 200℃.h^{-1}). One spectrum is also provided for the uncharged specimen, which contains only hydrogen related to the irreversible trap. Observing all the other spectra, a peak at around 100℃ is visible. This peak is visible at heating rates of 100℃.h^{-1} and 200℃.h^{-1} and may be issued from desorption of hydrogen contained in lattice and reversible traps. At a higher temperature, a non-negligible part of the total hydrogen is highly stabilized at around 450℃ and shows the plateau at 450℃ or higher.

Figure 6 corresponds to the results of the same experiment performed on the heat-treated condition. This figure shows similar spectra to the as-received one. The difference resides in the shape of the peak located at 110℃ and the plateau at a higher temperature. The shape of the first peak (dissymmetry) in this case suggests the superposition of a secondary peak with closer energy to the first one. These results are concordant with the reversible trap observed in Figure 4. In parallel, the ascending plateau at higher temperatures suggests some pollution of the specimen intrinsic to the apparatus. The plateau itself is then judged as irrelevant to interpret.

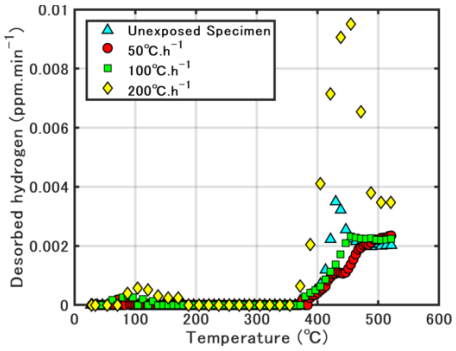

Figure 5 TDS spectra relative to the as-received condition. Three heating rates are presented: 50℃.h^{-1}, 100℃.h^{-1}, 200℃.h^{-1}. The spectrum of the unexposed specimen has also been included.

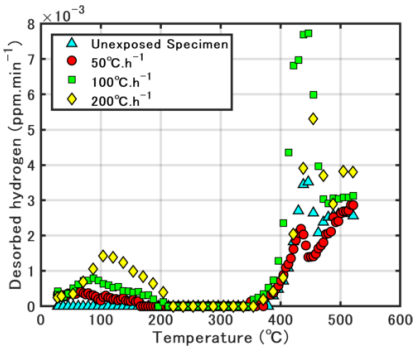

Figure 6 TDS spectra relative to the heat-treated condition. Three heating rates are presented: 50℃.h^{-1}, 100℃.h^{-1}, 200℃.h^{-1}. The spectrum of the unexposed specimen has also been included.

In both Figures 5 and 6, the actual amount of hydrogen differs from the Figures 3 and 4 because of the different dimensions of the specimen. Therefore, the signal is different and weaker in the case of the TDS experiment compared to the diffusion measurements.

Figure 7 presents the Choo-Lee's representation of all the peaks in both as-received (a) and heat-treated (b) conditions. The linear fitting, illustrated by the dashed line, suggests that some of the peaks are to be discarded (the spectra are also relatively noisy for low energy peaks). It has therefore been chosen to timely discard some spectrum in which the desorption signal was excessively noisy.

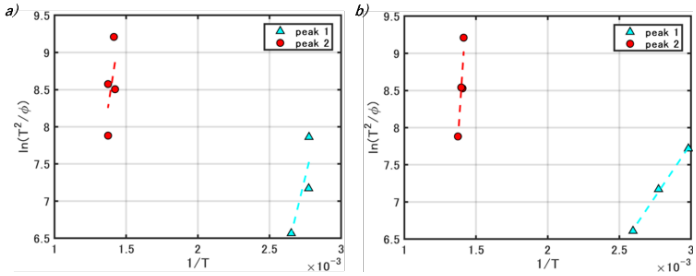

Figure 7 Choo-Lee's representation of the results for as-received condition (a) and heat-treated condition (b). The results of the linear fitting are given by the dashed line.

The energies calculated from the Choo-Lee's method are as follows. For the as-received condition, the first peak barely observed for the specimen at 50℃.h^{-1} (since the interpretation of this data may not be sufficiently accurate, this point is discarded). For the other cases, the signal is quite weak. In consequence, the resulting trap energy being inaccurate, it has been chosen to discard these results. The activation energy for the peak at 430℃ in Figure 5 corresponds to 107 kJ.mol^{-1}. For the heat-treated condition, the activation energies for the peaks located around 110℃ and 430℃ in Figure 6 correspond to 26.2 kJ.mol^{-1} and 165.8 kJ.mol^{-1} respectively. The spectra observed at higher temperatures (400℃ or higher) are superposed in both steels. Therefore, it is assumed that the trap is not altered by heat treatment so the value of these peaks could be averaged. The validity of these energies is then later discussed according to the deconvoluted signal.

NUMERICAL SIMULATIONS

Method

Modelling of the hydrogen diffusion and desorption has been carried out by use of the FEM program WELDSIMS (Fjær et al. 2013) developed

for the computing of temperatures, stresses and hydrogen concentration during welding. The diffusion of hydrogen is governed by Fick's law. The flux density of hydrogen **J** is computed from the gradient in the normalised concentration $\phi = C_L/s$ and the gradient in pressure ∇p. Here, C_L is the concentration of diffusible (lattice) hydrogen, s is the solubility, D is the diffusivity, and κ_p is a stress factor.

$$\mathbf{J} = -sD\left(\nabla\phi + \kappa_p \nabla p\right) \tag{2}$$

In the TDS and diffusion tests, stresses and gradients in solubility can be assumed to be negligible. The conservation equation can then be written as

$$\frac{\partial C}{\partial t} = \frac{\partial C_L}{\partial t} + \frac{\partial C_T}{\partial t} = \nabla \cdot \left(D \nabla C_L\right) \tag{3}$$

where the total concentration of hydrogen C has been written as the sum of the concentration in lattice sites C_L and the concentration in traps C_T. The hydrogen concentration in traps is assumed to be in thermodynamically equilibrium with the lattice concentration. According to Oriani (1970), this condition can be expressed by the difference in energy between a trap site and a lattice site ΔE_T, and the occupancy in lattice cites $\theta_L = C_L/N_L$ and in traps $\theta_T = C_T/N_T$.

$$\frac{\theta_T}{\theta_L\left(1-\theta_T\right)} = \exp\left(\frac{\Delta E_T}{RT}\right) = K_T \tag{4}$$

Here, the approximation $\theta_L << 1$ has been used. N_L and N_T are respectively the density of lattice sites (5.2×10^{29} m^{-3}) and trap sites, R is the gas constant, T is the temperature and K_T is the equilibrium constant. The concentration of hydrogen in traps can then be expressed by

$$C_T = \frac{N_T C_L}{C_L + N_L/K_T} \tag{5}$$

Including the effect of varying temperature, the time derivative of C_T can be expressed by:

$$\frac{\partial C_T}{\partial t} = \frac{\partial}{\partial C_L}\left(\frac{N_T C_L}{C_L + N_L/K_T}\right)\frac{\partial C_L}{\partial t} + \frac{\partial}{\partial T}\left(\frac{N_T C_L}{C_L + N_L/K_T}\right)\frac{\partial T}{\partial t} \tag{6}$$

Allowing for co-existence of several types of traps with different trap binding energies $\Delta E_T^{(i)}$ (Dadfarnia et al.), one obtains by inserting into the conservation equation

$$\left(1 + \sum_i \frac{N_T^{(i)} N_L K_T^{(i)}}{\left(K_T^{(i)} C_L + N_L\right)^2}\right)\frac{\partial C_L}{\partial t} = \nabla \cdot \left(D \nabla C_L\right) + \sum_i \frac{N_T^{(i)} N_L K_T^{(i)} \Delta E_T^{(i)} C_L}{RT^2\left(K_T^{(i)} C_L + N_L\right)^2}\frac{\partial T}{\partial t} \tag{7}$$

Below, Figure 11 shows values of the quantity D^*/D where D^* is defined by

$$D^* = D \Bigg/ \left(1 + \sum_i \frac{N_T^{(i)} N_L K_T^{(i)}}{\left(K_T^{(i)} C_L + N_L\right)^2}\right) \tag{8}$$

When the common assumption $\theta_T << 1$ is valid, D^* is independent of the lattice concentration and corresponds to the effective diffusivity.

The lattice diffusivity D is expressed by

$$D = D_0 \exp\left(-Q/RT\right) \tag{9}$$

where D_0 and Q are respectively given the values 1.0–2.52×10^{-7} m^2/s and 6.70-7.12 kJ/mol in the temperature range 50–550°C (Kiuchi and McLellan, 1983).

As it turned out to be difficult to identify peaks in the TDS spectra for as-received material, only tests on heat treated material has been analysed by numerical simulations. In the simulations of the diffusivity tests, a 2D axisymmetric solution domain with 2500 elements was applied. The simulations of the TDS tests, were carried out on a 1D domain with 400 elements involving one half of the thickness.

The hydrogen charging and a rest period was accounted for. In order to obtain a reasonable agreement with the measurements, it was necessary to tune the duration of the rest period in the simulation. At the time the heating of the samples started from a temperature of 25°C, the lattice concentration of hydrogen in the centre of the test specimen was respectively ca 0.0005 ppm in the simulation of the TDS tests and ca 0.02 ppm in the simulations of the diffusion tests.

The temperature evolution was governed by a time dependent boundary condition. When solving the hydrogen diffusion problem, a mass transfer coefficient and an equilibrium surface concentration of 1×10^{-10} ppm kept the boundary concentration below 0.1 ppb.

Trap densities and trap energies fitted to match the experimental data from both the diffusion tests and the TDS tests are listed in Table 5.

Table 5 Trap data applied in simulations.

Trap type	I	II	III	IV
Trap energy (kJ/mol)	20.0	57.5	69.0	120.0
Trap density (m^{-3})	2.37×10^{27}	1.0×10^{23}	5.0×10^{22}	7.0×10^{23}

Results and comparison with experiments

In general, the computed hydrogen desorption from the simulations of the diffusion tests at 50°C and 100°C is in Figure 8 seen to match the experimental results very well. It is however difficult to achieve an exact agreement with the measurements during the start of the experiment when the sample is heated from room temperature. In addition, the peaks in the desorption curves when the temperature pass ca. 150 ℃ is somewhat higher in the simulations than in the experiments. The desorption rate from the simulation of the TDS experiments shown in Figure 9(a) are somewhat lower than the experimental values shown in Figure 6. The position of the peaks at temperatures below 300°C and the relative magnitude of desorption for the various heating rates is however in a good agreement with the experiments. The peak associated with the high energy trap obtained when the temperature pass 400°C is strongly underestimated in the simulation of the TDS experiments, whereas the same set of trap data in the model gives a quite good agreement with the corresponding peak seen in the spectra from the diffusion experiments.

In order to identity the significance of the different trap types with respect to the computed TDS spectrum, a simulation omitting the traps of type III and IV and another simulation including only traps of type I is compared with the simulation of the test with a heating rate of 200°C/s that includes all 4 types of traps. The traps type III and IV is seen not to affect the results before the temperature reaches 100°C. One can assume that the high energy of these traps will cause these traps to be fully occupied for lower temperatures. With only traps of type I there is hardly seen any peak in the computed TDS spectrum. The predicted diffusion at room temperature is in this case so high that the decay in the desorption rate due to loss of diffusible hydrogen is predicted to be almost as high as the increase in desorption rate due to a lower trap occupancy and higher diffusivity when the temperature starts to increase. One could also notice that the traps of type II (57.5 kJ/mol) has a very small influence on the predicted desorption rate at the beginning of the test.

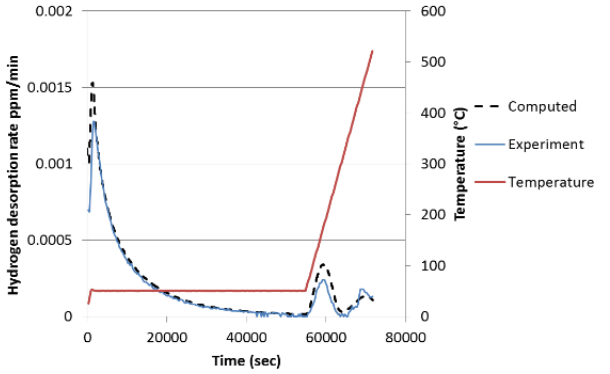

(a)

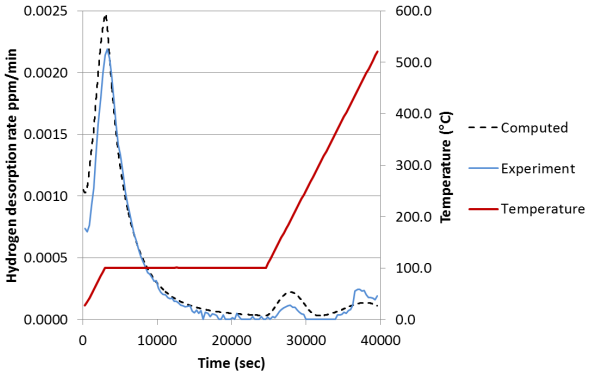

(b)

Figure 8 Comparison of experimental and computed hydrogen desorption rate from tests involving diffusion at (a) 50°C and (b) 100°C

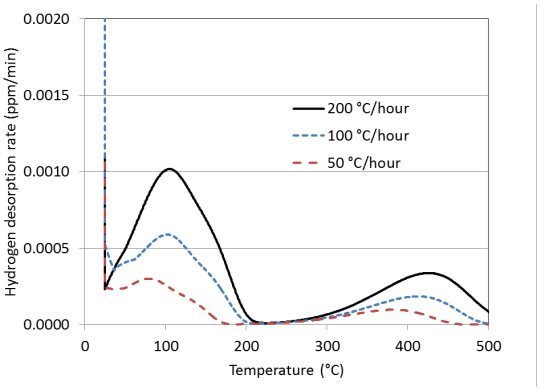

(a)

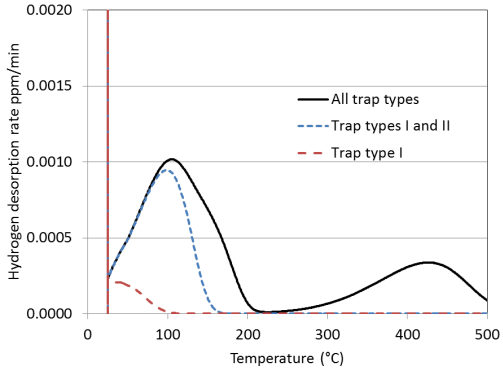

(b)

Figure 9 Computed hydrogen desorption rate in the TDS experiments. (a) Results for different heating rates (b) Results from simulations of the TDS experiments with a heating rate of 200°C/s showing the significance of the different types of traps.

DISCUSSION

Diffusion coefficient

The experiments have shown that the hydrogen diffusivity of the heat-treated condition is lower than that of the as-received one. In addition, both hydrogen diffusivities are lower than the lattice hydrogen diffusivity and the activation energies for hydrogen diffusivity are smaller than that in lattice diffusion (6 kJ.mol^{-1}, Skjellerudsveen et al.). This suggests that reversible trap sites with low energy affect the hydrogen diffusivity of both steels. As shown in Figure 1, the microstructure evolves from ferrite to a mix of bainite and martensite. Thus, different states (types and density) of reversible trap sites between the as-received and heat-treated conditions are considered to cause their different hydrogen-diffusion properties.

Hydrogen trapping

The comparison of desorption spectra shows some strong similarities for the lowest and the highest temperatures. The first peak around 110℃ is observable in both steels. It is suggested that the first peak is attributed to a reversible trap with low energy and the hydrogen related to this peak dominates the hydrogen diffusivity. Although the activation energy of the first peak (26.2 kJ.mol^{-1}) is not necessarily consistent with that of the hydrogen diffusivity (15.6 kJ.mol^{-1}), this inconsistency may be accepted considering noisy data used for the Choo-Lee's method. In contrast, some different trapping properties of the as-received and heat-treated conditions are pointed out. The presence of a new reversible trap site after 110℃ as well as the plateau observable until the end of the test proves that some sites have been generated by the normalization and quenching processes.

To characterize the new reversible trap site after 110℃, the signal is post-treated. A deconvolution for 100℃.h^{-1} and 200℃.h^{-1} is done supposing a gaussian response of the system. Figure 10 shows the deconvoluted spectra for 100 ℃.h^{-1} (a) and 200 ℃.h^{-1} (b). Experimental data is represented with marks. Each peak is plotted using dashed lines. The first peak (black) is common to both state. The second peak (blue) correspond to the reversible trap specific to the heat-treated case. The peaks 3 (magenta) and 4 (red) are identified as irreversible traps. The test has been aborted at 520℃ for accuracy reasons. Therefore, the quantitative aspects linked to peak 4 are refutable. The cumulated spectra (sum of the four peaks) is given by the solid line and concords with experiment. Reading Figure 10-a), the first peak is located at 88℃ and the second at 121℃. In the same way, the Figure 10-b) locates these peaks at 112℃ and 138℃ respectively. Using the Choo-Lee's method, the energy of the first peak is exactly the same as determined from Figure 7. The energy of the newly created reversible trap is 49.2 kJ.mol^{-1}. It is considered that this trap site also affects the hydrogen diffusion, causing a slight difference in the activation energy of hydrogen diffusivity between the as-received and heat-treated conditions. The energies resulting from the irreversible peaks are also concordant with the previous evaluation.

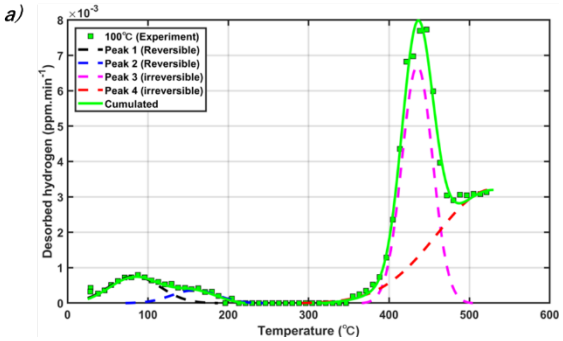

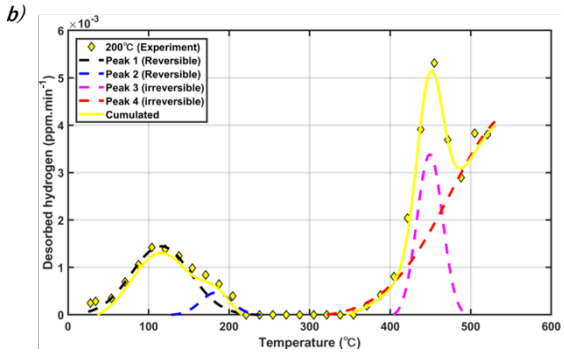

Figure 10 Deconvolution of the TDS spectra of the heat-treated material a) refers to the 100℃.h^{-1} condition and b) to the 200℃.h^{-1} condition.

In parallel, the amount and the proportion of hydrogen within the irreversible traps is decreased by the heat treatment. In other words, this means that most of the hydrogen is contained in the reversible traps. The analysis of the high temperature plateau has not been conducted in the present study. To access all the energies relative to irreversible traps, the signal remains to be deconvoluted to be fit by adequate distributions.

Several trapping energies are available in literatures. Usually, the trapping energies of crystallographic defects is lower than precipitate interface. Hence, the trap binding energies of hydrogen range from 17 kJ.mol^{-1} to 61 kJ.mol^{-1} for grain boundaries and martensitic interfaces (Choo and Lee; Ono and Meshii; Asaoka et al.; Wei et al.; Li et al.), from 0 kJ.mol^{-1} to 59 kJ.mol^{-1} for dislocations (Oriani; Hill and Johnson; Kumnick and Johnson; Takai) and from 50 kJ.mol^{-1} up to 143 kJ.mol^{-1} for various precipitates (Fe_3C excluded) (Lee and Lee; Podgurski and Oriani; Wei et al.; Wallaert et al.). Although the trap binding energy for the dislocations shows a large variation, Takai mentions that the trap binding energies ranging from 0 to 20 kJ.mol^{-1} are attributed to the elastic field of the dislocations and the binding energy of 59 kJ.mol^{-1} is attributed to the dislocation cores (TAKAI). The comparison of microstructures in Figure 1 indicates the presence of cementite in both materials but with a different arrangement. Therefore, the irreversible traps are more likely to be attributed to metal-Fe_3C interfaces since this signal is detected in both steels. The trapping site with the activation energy of 26.2 kJ.mol^{-1} is observed from both as-received and heat-treated conditions and therefore, it is considered to be attributed mainly to the elastic field of the dislocations. In contrast, the activation energy of 49.2 kJ.mol^{-1} is significant only for the heat-treated condition. Considering the difference in microstructures between the as-received and heat-treated conditions, this trapping site may be mainly attributed to the martensitic interfaces.

Numerical simulations

Analyses of TDS tests is suggested to be handled by using computational methods, as Choo-Lee's method only consider de-trapping and not diffusion or re-trapping (Bhadeshia). Two different modelling approaches are used. Numerical analyses based on Oriani's equilibrium model, as in the modelling presented here, (Song;Yamaguchi), and analyses based on the kinetic model by McNabb and Foster (Wei 2012; Enomoto). If a large pre-exponential factor is used in the expression for de-trapping in the kinetic model, the models will give corresponding results (Krom, Song). When the assumption of low trap occupancy (θ_T<<1), it can be shown that the parameters in Kissinger's formula on which the Choo-Lee's method is based can be derived from the effective diffusivity and the dimension of the sample (Wei 2012).

The definition of D^* above corresponds to the common definition of the efficient diffusivity D_{eff} (see e.g. Krom). However, its value will only be independent of the lattice concentration if the occupancy of all types of traps is either very low or close to 1. In Figure 11, D^* divided by the lattice diffusivity is shown as a function of temperature for different values of the lattice concentration. For temperatures below 80°C and a lattice concentration above 0.01 ppm, D^* is independent of the lattice concentration. This corresponds to a situation where only the low energy traps (type I) affect the diffusivity whereas traps with higher energy are fully occupied. These conditions with a low temperature and high C_L is the most relevant for oil and gas applications, and for these conditions a good agreement is found between model and the diffusion experiments. However, in the case of a higher temperature or a lower lattice concentration, the occupancy of the traps with energy 57.5 kJ/mol (type II) becomes significantly lower than 1, see Figure 12, and D^* becomes lower as also these traps becomes active slowing down the diffusion. For even lower values of the lattice concentration, also the traps of type II and IV will be only partly filled, and D^* or the effective diffusivity becomes even lower. With the set of trap data applied here for the heat treated X70 steel, the low trap occupancy approximation is seen not to be valid when either the lattice concentration becomes low or the temperature becomes high. This can explain why there is a discrepancy between the trap energies found by the Choo-Lee's method and the trap energies identified by the numerical analyses. When comparing the result from the trap activation energy E_a derived by the Choo-Lee's method and the trap energy used in the numerical modelling ΔE_T, one should note that $E_a = \Delta E_T + Q$ where Q is the energy associated with the lattice diffusion (Choo).

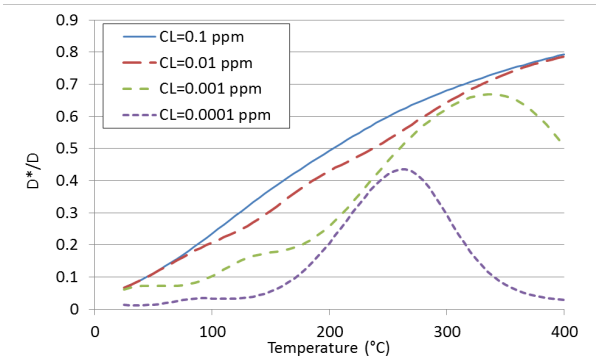

Figure 11 D^*/D as a function of temperature for different values of the lattice concentration

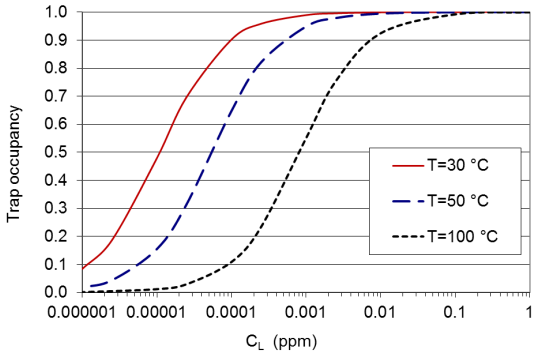

Figure 12 Trap occupancy for traps with energy 57.5 kJ/mol as function of lattice concentration at some selected temperatures.

CONCLUSIONS

1. Hydrogen diffusivity of the API X70 steel has been measured at temperatures ranging from 30 ℃ to 170 ℃. The hydrogen diffusivity of the heat-treated condition was lower than that of the

as-received one state. Both diffusivities were lower than the lattice hydrogen diffusivity and therefore, the different diffusion properties between the as-received and heat-treated conditions are considered to be caused by different states (types and density) of trap sites related to their microstructures.

2. A reversible trap site with an activation energy of 26.2 $kJ.mol^{-1}$ and an irreversible trap site with an activation energy of >100 $kJ.mol^{-1}$ were observed from both as-received and heat-treated condition. In contrast, a reversible trap site with an activation energy of 49.2 $kJ.mol^{-1}$ was observed only from the heat-treated condition. The contribution of the trap site with 49.2 $kJ.mol^{-1}$ to the hydrogen diffusivity may be one of reasons why the hydrogen diffusivities of the as-received and heat-treated conditions were not the same.
3. Following literatures and microstructures, it was suggested that the trapping sites with the activation energies of 26.2 $kJ.mol^{-1}$, 49.2 $kJ.mol^{-1}$, and >100 $kJ.mol^{-1}$ were mainly attributed to the elastic field of dislocations, martensitic interfaces, and metal-Fe_3C interfaces, respectively.
4. The numerical modelling based on the assumption of equilibrium between hydrogen in traps and hydrogen in lattice is seen to provide a good fit to the experimental data. It confirms the major findings from the analytical methods that this steel contains a combination of low energy traps that dominates the hydrogen diffusion at high concentrations, reversible traps with somewhat higher energy, and irreversible traps.

ACKNOWLEDGEMENTS

This work is performed within the project Knowledge Basis for Repair Contingency of Pipelines (234110/E30) funded by the Research Council of Norway, Statoil, Gassco, Technip, EFD Induction and POSCO.

REFERENCES

Asaoka, T., et al. “Quantitative Study of Trapping Characteristics of H in a Fe-0. 15 per Cent Ti Ferrite by High-Resolution Autoradiography and During Degassing at High Temperatures.” *Scr. Metall.*, vol. 11, no. 6, 1977, pp. 467–72.

Bhadeshia, HKDH., 2016, "Prevention of Hydrogen Embrittlement in Steels", *ISIJ International*, vol. 56, pp. 24-36.

Choo, W. Y., and J. Y. Lee. “Thermal-Analysis of Trapped Hydrogen in Pure Iron.” *Metallurgical Transactions a-Physical Metallurgy and Materials Science*, vol. 13, no. 1, 1982, pp. 135–40, doi:Doi 10.1007/Bf02642424.

Dadfarnia, M, Sofronis, P,Neeraj, T, (2011), “Hydrogen interaction with multiple traps: Can it be used to mitigate embrittlement?”, I*nternational Journal of Hydrogen Energy*, 36, 10141-10148.

Enomoto, M,Hirakami, D, (2015), "Influence of Specimen Thickness on Thermal Desorption Spectrum of Hydrogen in High Strength SCM435 Steel", *ISIJ International*, vol. 55, pp. 2492-2498.

Fjær, HG, Aas, SK, Olden, V, Lindholm D, and Akselsen, OM (2013). ”Simulation of Multipass Welding of a Steel Pipe Including Modelling of Hydrogen Diffusion and Fracture Mechanics Assessment,” *Mathematical Modelling of Weld Phenomena 10*, Verlag der Technischen Universität Graz, pp 371-399.

Hill, M. L., and E. W. Johnson. “Hydrogen in Cold Worked Iron-Carbon Alloys and the Mechanism of Hydrogen Embrittlement.” *Transactions of the Metallurgical Society of AIME*, vol. 215, 1959, pp. 717–25.

Kiuchi, K.,McLellan, RB, 1983, The solubility and diffusivity of hydrogen in well-annealed and deformed iron, A*cta Metallurgica*, vol. 31, pp. 961-984.

Krom, AHM.,Bakker, A, (2000), Hydrogen Trapping Models in Steel, *Metallurgical Transactions*, vol. 31B, pp. 1475-1482.

Kumnick, A. J., and H. H. Johnson. “Deep Trapping for Hydrogen Iron.” *Acta Metallurgica*, vol. 28, 1980, pp. 33–39.

McNabb, A, Foster, PK, (1963) "A new analysis of the diffusion of hydrogen in iron and ferritic steels" , *Trans. AIME*, Vol. 227, pp 618–627.

Lee, H. G., and Jai-Young Lee. “Hydrogen Trapping by TiC Particles in Iron.” *Acta Metallurgica*, vol. 32, no. 1, Elsevier, 1984, pp. 131–36.

Li, Daoming, et al. “Hydrogen Trap States in Ultrahigh-Strength AERMET 100 Steel.” *Metallurgical and Materials Transactions A*, vol. 35, no. 3, 2004, pp. 849–64, doi:10.1007/s11661-004-0011-1.

Ono, K., and M. Meshii. “Hydrogen Detrapping from Grain Boundaries and Dislocations in High Purity Iron.” *Acta Metallurgica et Materialia*, vol. 40, no. 6, Elsevier, 1992, pp. 1357–64.

Oriani, Richard A. “The Diffusion and Trapping of Hydrogen in Steel.” *Acta Metallurgica*, vol. 18, no. 1, Elsevier, 1970, pp. 147–57.

Podgurski, H. H., and R. A. Oriani. “Nitrogenation of Fe-Al Alloys. III: Absorption of Hydrogen in Nitrogenated Fe-Al Alloys.” *Metallurgical and Materials Transactions B*, vol. 3, no. 8, Springer, 1972, pp. 2055–63.

Skjellerudsveen, Magnus, et al. “Effect of Microstructure and Temperature on HydrogenDiffusion and Trapping in X70 Grade Pipeline Steel and itsWeldments.” *EuroCorr 2010, Moskva*, 2010.

Song, EJ, Suh, D-W, Bhadeshia, HKDH, (2013), "Theory for hydrogen desorption in ferritic steel", *Computational Materials Science*, vol. 79, pp. 36-44.

TAKAI, Kenichi. “Hydrogen Existing States in Metals.” *Transactions of the Japan Society of Mechanical Engineers Series A*, vol. 70, no. 696, 2004, pp. 1027–35, doi:10.1299/kikaia.70.1027.

Wallaert, Elien, et al. “Thermal Desorption Spectroscopy Evaluation of the Hydrogen-Trapping Capacity of NbC and NbN Precipitates.” *Metallurgical and Materials Transactions A*, vol. 45, no. 5, Springer, 2014, pp. 2412–20.

Wei, F. G., et al. “Precise Determination of the Activation Energy for Desorption of Hydrogen in Two Ti-Added Steels by a Single Thermal-Desorption Spectrum.” *Metallurgical and Materials Transactions B*, vol. 35, no. 3, Springer, 2004, pp. 587–97.

Wei, F-G, Enomoto, M,Tsuzaki, K, (2012), "Applicability of the Kissinger’s formula and comparison with the McNabb–Foster model in simulation of thermal desorption spectrum", *Computational Materials Science*, vol. 51, pp. 322-330.

Yamabe, Junichiro, Tohru Awane, et al. “Elucidating the Hydrogen-Entry-Obstruction Mechanism of a Newly Developed Aluminum-Based Coating in High-Pressure Gaseous Hydrogen.” *International Journal of Hydrogen Energy*, vol. 40, no. 32, Elsevier Ltd, 2015, pp. 10329–39, doi:10.1016/j.ijhydene.2015.06.023.

Yamabe, Junichiro, Osamu Takakuwa, et al. “Hydrogen Diffusivity and Tensile-Ductility Loss of Solution-Treated Austenitic Stainless Steels with External and Internal Hydrogen.” *International Journal of Hydrogen Energy*, vol. 42, no. 18, Elsevier Ltd, 2017, pp. 13289–99, doi:10.1016/j.ijhydene.2017.04.055.

Yamabe, Junichiro, Tohru Awane, et al. “Investigation of Hydrogen Transport Behavior of Various Low-Alloy Steels with High-Pressure Hydrogen Gas.” *International Journal of Hydrogen Energy*, vol. 40, no. 34, Elsevier Ltd, 2015, pp. 11075–86, doi:10.1016/j.ijhydene.2015.07.006.

Yamaguchi, T, Nagumo, M, (2003), “Simulation of Hydrogen Thermal Desorption under Reversible Trapping by Lattice Defects”*, ISIJ International,* vol. 43, pp. 514-519.